

Submitted to ApJ

# Environmental effects on the growth of super massive black holes and AGN feedback

Min-Su Shin

*Princeton University Observatory, Peyton Hall, Princeton, NJ 08544-1001, USA*

Jeremiah P. Ostriker

*Princeton University Observatory, Peyton Hall, Princeton, NJ 08544-1001, USA**Institute of Astronomy, University of Cambridge, Madingley Road, Cambridge CB3 0HA, UK*

Luca Ciotti

*Department of Astronomy, University of Bologna, via Ranzani 1, I-40127, Bologna, Italy*

## ABSTRACT

We investigate how environmental effects by gas stripping alter the growth of a super massive black hole (SMBH) and its host galaxy evolution, by means of 1D hydrodynamical simulations that include both mechanical and radiative AGN feedback effects. By changing the truncation radius of the gas distribution ( $R_t$ ), beyond which gas stripping is assumed to be effective, we simulate possible environments for satellite and central galaxies in galaxy clusters and groups. The continuous escape of gas outside the truncation radius strongly suppresses star formation, while the growth of the SMBH is less affected by gas stripping because the SMBH accretion is primarily ruled by the density of the central region. As we allow for increasing environmental effects - the truncation radius decreasing from about 410 to 50 kpc - we find that the final SMBH mass declines from about  $10^9$  to  $8 \times 10^8 M_\odot$ , but the outflowing mass is roughly constant at about  $2 \times 10^{10} M_\odot$ . There are larger changes in the mass of stars formed, which declines from about  $2 \times 10^{10}$  to  $2 \times 10^9 M_\odot$ , and the final thermal X-ray gas, which declines from about  $10^9$  to  $5 \times 10^8 M_\odot$ , with increasing environmental stripping. Most dramatic is the decline in the total time that the objects would be seen as quasars, which declines from 52 Myr (for  $R_t = 377$  kpc) to 7.9 Myr

(for  $R_t = 51$  kpc). The typical case might be interpreted as a red and dead galaxy having episodic cooling flows followed by AGN feedback effects resulting in temporary transitions of the overall galaxy color from red to green or to blue, with (cluster) central galaxies spending a much larger fraction of their time in the elevated state than do satellite galaxies. Our results imply that various scaling relations for elliptical galaxies, in particular, the mass ratio between the SMBH and its host galaxy, can have dispersions due to environmental effects such as gas stripping. In addition, the simulations also suggest that the increase in AGN fraction in high-redshift galaxy clusters might be related to environmental effects which shut down the SMBH mass accretion in satellite galaxies and reduce their AGN activity.

*Subject headings:* galaxies: active — galaxies: elliptical and lenticular — galaxies: ISM — galaxies: nuclei

## 1. Introduction

The role of the environment in galaxy evolution has been suggested in various forms which strip out gas from a galaxy and goes all the way back to the early suggestion by Spitzer & Baade (1951). For example, the ram pressure of the intracluster medium is a possible way to strip out gas from falling galaxies partially or completely in galaxy clusters and to stop the supply of cold gas for star formation (Gunn & Gott 1972; Larson et al. 1980; Takeda et al. 1984; Gaetz et al. 1987; Begelman & Fabian 1990; Abadi et al. 1999; Domainko et al. 2006; Tonnesen & Bryan 2008; Kapferer et al. 2009). Other possible processes include thermal evaporation and viscous stripping (Cowie & Songaila 1977; Livio et al. 1980; Nulsen 1982; Nepveu 1985; Valluri & Jog 1990; Roediger & Brüggen 2008). The combined gas loss by these different types of destruction effects is expected in galaxy clusters or groups (Stevens et al. 1999; Quilis et al. 2000; Toniazzo & Schindler 2001; Kawata & Mulchaey 2008; McCarthy et al. 2008; Smith et al. 2009). Tidal stripping can also play an important role in changing the gas and stellar mass of cluster or group galaxies (Merritt 1983; Moore et al. 1999; D’Ercole et al. 2000).

Recent multi-wavelength observations have proved the loss of gases in cluster or group elliptical galaxies. In some elliptical galaxies, diffuse X-ray emitting gases show a long tail structure which can be explained by ram pressure stripping (e.g. Kim et al. 2008a; Randall et al. 2008). Infrared observations also revealed dust emissions that can be from gas stripped from elliptical galaxies (e.g. White et al. 1991).

A central galaxy which hosts satellite galaxies in groups and clusters <sup>1</sup> exhibits different features compared to satellites which can be affected by the various stripping processes. Because the central galaxy sits near the bottom of a deep gravitational potential well, its hot gas halo is much larger than those of satellites (e.g. Sun et al. 2005), and it is not surprising that it shows signatures of cooling flows in some cases (see Fabian 1994; Reiprich et al. 2004, for a review).

Quite obviously, the differences in the stellar populations between satellites and central galaxies also have been studied, being relevant to our understanding of the environmental effects. For example, red satellite galaxies are redder than central galaxies of the same stellar mass (van den Bosch et al. 2008). Many central galaxies in clusters display either recent star formation or ongoing star formation which may be related to the cooling flow from their hot gas halos (Cardiel et al. 1998; Rafferty et al. 2006; Bildfell et al. 2008; O’Dea et al. 2008; Pipino et al. 2009) and which would be of reduced significance for satellite galaxies. Satellite galaxies in galaxy clusters seem to gradually lose of their gas by environmental effects and to truncate star formation, comparing their current and past star formation with those of field galaxies (e.g. Balogh et al. 1999).

Differences in the properties of a central super massive black hole (SMBH) and its activity are expected between central and satellite galaxies, when considering the strong correlation between spheroidal galaxies and their SMBHs. The ratio of the SMBH mass over the spheroidal mass is found to be about  $10^{-3}$  with a small dispersion for a large mass range in local galaxies (Kormendy & Richstone 1995; Magorrian et al. 1998; Ferrarese & Merritt 2000; Gebhardt et al. 2000; Ferrarese 2002; Yu & Tremaine 2002; Marconi & Hunt 2003; Häring & Rix 2004). If the growth of stellar mass and SMBH mass are coupled to the same kind of environmental effects, it is natural to conclude that the properties of SMBHs in satellite galaxies must be somewhat different from those of central galaxies. As we emphasized in our previous papers (Ciotti et al. 2009a, hereafter Paper I; Shin et al. 2010, hereafter Paper II) the self-regulated growth of SMBHs is profoundly dependent on how the accretion energy is converted to heat the ambient interstellar medium and how frequently and quickly the feedback process is ignited in the right place: we called these two key issues *the problem of energy conversion* and *the timing problem*. One would expect that the environmental effects might induce differences in the frequency of AGN feedback and the growth of the SMBHs by varying the conditions of the self-regulation process.

---

<sup>1</sup>A primary galaxy accreting satellites in group and cluster environment corresponds to the brightest cluster galaxy (BCG) in this paper. For isolated galaxies, the term *central galaxy* is correspondent to a primary galaxy which hosts satellites (e.g. Ann et al. 2008). In this paper, the key feature to define satellites is that they experience gas stripping which is strong enough to affect their evolution.

In this paper, we tackle the issue of environmental effects on the coevolution of the SMBH and its host galaxy by simulating the evolution of a galaxy in hydrodynamical models with a simplified setup of different environments. Although there is no current systematic investigation of the SMBH mass and AGN activity for separating satellite and central galaxies, the theoretical prediction from our simulations can be used to constrain the hypothesis of the coevolving SMBH and its host galaxy and the connection to environmental effects.

This paper is organized as follows. In Section 2, we describe the models and the simulations. The results are presented in Section 3. Discussion and conclusions follow in Section 4.

## 2. Simulations

We adopt as a basic model the B3<sup>w</sup> model that is given in Ciotti et al. (2010, hereafter Paper III). This model incorporates both radiative and mechanical feedback effects from the central SMBH in 1D hydrodynamic simulations. The basic input physics is fully described in Paper I and II. Here, we summarize the main ingredients of simulations and explain how to implement different environments.

We setup an initial galaxy following observed properties of local elliptical galaxies. First, the stellar mass is distributed to be consistent with Faber-Jackson relation and the Fundamental Plane, assuming an identical amount of stellar and dark matter mass within the half-mass radius (e.g., Tortora et al. 2009); all the relevant dynamical and structural properties of the models are given in Paper III. Second, the initial mass of the central SMBH  $M_{\text{BH}}$  is 0.001 of the initial stellar mass  $M_*$ . In all simulations, we set  $M_* = 2.9 \times 10^{11} M_\odot$ , the effective radius  $R_e$  is 6.9 kpc, and the central aperture velocity dispersion is 260 km/s (see Appendix for different initial velocity dispersions and their effects). Therefore, in our simulations, we are tracing the late evolution of ellipticals after the initial epoch of formation, i.e., of major growth of both the stellar component and of the central SMBH.

In addition to passive stellar feedback effects, i.e. mass losses and type Ia supernovae, the simulations include both radiative and mechanical feedback due to the SMBH as well as secondary stellar feedback effects from recurrent star formation. As discussed in Paper I, II, and III, the observational constraints such as the mass ratio between the SMBH and its host galaxy, the X-ray luminosity from hot diffuse gas, the quasar lifetime, and the recent star formation fraction, are better matched by simulations which include both feedback modes than simulations restricted to purely radiative or purely mechanical feedback models (see Begelman 2004, for a review of various forms of feedback). Radiative feedback affects

the ambient medium around the SMBH via radiative heating mediated by photoionization, Compton heating, and radiation pressure. These can be effective forms of AGN feedback over a large spatial range depending on a frequency range of AGN radiation (Sazonov et al. 2004, 2005; Fabian et al. 2006; Ciotti & Ostriker 2007). Meanwhile, the typical form of mechanical feedback is represented by the interaction of nuclear winds and jets from accreting SMBHs which ultimately heat up the surrounding interstellar medium with maximum effectiveness in  $r \ll 0.1$  kpc (Tabor & Binney 1993; Binney & Tabor 1995; Begelman 2004; Veilleux et al. 2005; Springel et al. 2005a; Königl 2006; Johansson et al. 2009).

In our models, we control the strength of radiative feedback with the parameter  $\epsilon_0$  which is related to the radiative efficiency  $\epsilon_{\text{EM}}$  that determines the bolometric accretion luminosity from the SMBH

$$L_{\text{BH}} = \epsilon_{\text{EM}} \dot{M}_{\text{BH}} c^2 \quad (1)$$

by

$$\epsilon_{\text{EM}} = \epsilon_0 \frac{A \dot{m}}{1 + A \dot{m}}. \quad (2)$$

Equation 2 is a phenomenological implementation of the main features of the ADAF (Advection Dominated Accretion Flow) accretion (Narayan et al. 1996) with the rescaled SMBH accretion rate with respect to the Eddington accretion rate  $\dot{m} = \dot{M}_{\text{BH}}/\dot{M}_{\text{Edd}}$ . The parameter  $A$  is 100 as in Paper I and II. We use  $\epsilon_0 = 0.1$ , which is favored by observational constraints for luminous quasar phase, i.e. when  $\dot{m}$  is high (e.g. Soltan 1982)<sup>2</sup>.

The parameter  $\epsilon_{\text{w}}^{\text{M}}$  handles the mechanical efficiency of the AGN wind which is coupled to the bolometric accretion luminosity of AGN and affects the mass loss rate of gas by the wind (Kurosawa et al. 2009a). After the introduction of the normalized accretion luminosity with respect to the Eddington luminosity  $L_{\text{Edd}}$ ,

$$l \equiv \frac{L_{\text{BH}}}{L_{\text{Edd}}} = \frac{A \dot{m}^2}{1 + A \dot{m}}, \quad (3)$$

the mechanical efficiency of the AGN wind  $\epsilon_{\text{w}}$  is

$$\epsilon_{\text{w}} \equiv \frac{3\epsilon_{\text{w}}^{\text{M}}}{4} \frac{l}{1 + 0.25l}. \quad (4)$$

In this paper, we fix  $\epsilon_{\text{w}}^{\text{M}} = 3 \times 10^{-4}$  which is one of the explored models and suggested as the probable value in Paper III. The peak mechanical feedback efficiency  $\epsilon_{\text{w}}^{\text{M}}$  governs how much

---

<sup>2</sup>In Paper III, we also present models with  $\epsilon_0 = 0.2$ .

kinetic energy, momentum, and mass has to be deposited to the broad-line region, with the mass loss coefficient of the AGN wind (Kurosawa & Proga 2009b,c)

$$\eta_w \equiv \frac{3\eta_w^M}{4} \frac{l}{1 + 0.25l}. \quad (5)$$

where  $\eta_w^M = 1800\epsilon_w^M$  which is consistent with observational constraints on the velocity of the broad-line regions and the ionized absorption outflows in quasars (e.g. Krongold et al. 2007).

The important feature of our simulations is the boundary condition that mimics different environments having different strengths of gas stripping. In practice, this is accomplished by changing the position of the last grid point  $R_t$  (hereafter called "truncation radius") where outflow boundary conditions are imposed. We assume that gas escapes beyond the truncation radius as various destruction processes caused by the environment (principally, ram-pressure stripping) reduce the size of hot gas halo, but do not totally destroy it (Brighenti & Mathews 1999; Sun et al. 2005). There is no infall of gas from outside these radii.

The efficiency of gas stripping depends on both galaxy and intracluster medium properties (see Hester 2006, for discussions). The gravity from mass distribution in the galaxy competes with ram pressure which depends on the density of intracluster medium and relative velocity of galaxies with respect to intracluster medium. Therefore, the stripping strength can vary significantly depending on the complex combinations of galaxy models and the flows of intracluster medium toward galaxies, i.e. the orbits of galaxies and the properties of the intracluster medium.

Even though this setup of different environments is too simple and the symmetric stripping never happens in real conditions, it will help us to understand how environmental effects might affect galaxy evolution with AGN feedback. Simply, small values of  $R_t$  correspond to the satellite-like environment where gas stripping can be effective, while large values of  $R_t$  represent the environment of central galaxies which can keep a large amount of diffuse hot gas, practically without any substantial loss of gas (but without the confining effect of some external pressure, as for example, the intracluster medium of the center of a galaxy cluster).

We test ten different truncation radii for the same initial stellar mass and SMBH mass. As given in Table 1,  $R_t$  ranges from about 51 kpc to 413 kpc. This range corresponds to about 7 to 60  $R_e$ . Initially, all galaxies have the same density and temperature distribution of gas within the truncation radius. Therefore, when density and temperature distribution of hot gas is same in all cases at a certain time, the total X-ray luminosity emitted from the hot gas is expected to be lowest for the smallest truncation radius, i.e. Run 1. The spatial resolution of all runs is exactly the same despite the differences of the truncation radii, having different numbers of radial grids. The inner most grid point is placed at 2.5 pc from the center in all runs.

The simulation follows the evolution of a galaxy, which begins at the cosmic age 2 Gyr and stops at 14 Gyr, by solving the hydrodynamic equations of the gas, being supplemented by prescriptions for star formation and stellar feedback. Because the simulations begin at 2 Gyr, i.e. a redshift of  $z \sim 3.2$  for the LCDM cosmology with  $\Omega_m = 0.3$ ,  $\Omega_\lambda = 0.7$ , and  $H_0 = 70$  km/s/Mpc, it is assumed that a bulk of stellar mass is already established at the beginning epoch (Renzini 2006; van Dokkum et al. 2010).

As explained in our previous papers, the simulations are not meant to reproduce the cosmological context. Instead, we explore the physical link between the local small-scale physics around SMBHs and the global scale of a single galaxy during late evolutionary phases. In general, it is already difficult to achieve this dynamic range with the intricate prescriptions of AGN feedback, so that cosmological gas infall or galaxy merger/accretion are not implemented in our simulations (Di Matteo et al. 2008; Letawe et al. 2008). This limitation must be considered when interpreting our simulation results. However, the recent observations suggest that the final stage of fueling onto the SMBH is controlled primarily by the self-regulation process instead of large-scale episodic effects such as galaxy mergers (Grogin et al. 2005; Kollmeier et al. 2006; Li et al. 2008; Gabor et al. 2009; Silverman et al. 2009; Reichard et al. 2009). Moreover, in this paper we focus on effects by gas stripping only.

### 3. Results

#### 3.1. Evolution of models

In all computed models, the growth of the new stars and the SMBH is strongly regulated by how frequently active phases of SMBHs occur. At early times, all models are characterized by the accumulation of recycled gas and its cooling which finally results in the formation of new stars and almost simultaneous SMBH growth, with a strongly intermittent activity as shown in Figure 1. The coincident activity of star formation and SMBH accretion is consistent with blue colors of quasar-hosting elliptical galaxies at low and high redshifts and the recent star formation in AGN hosts (e.g. Jahnke et al. 2004; Sánchez et al. 2004).

The repetition of star formation episodes and the active SMBH phases is basically caused by self-regulation of AGN feedback, which heats up the cooling flow for star formation and suppresses fueling to the SMBH responding the cooling rate. The time intervals between the peaks of star formation rate  $\dot{M}_*$  and the central SMBH growth rate  $\dot{M}_{\text{BH}}$  become progressively longer and longer, even though the precise timing of the repetition varies in each run. This delay is the result of the decline of  $\dot{M}_*$  with cosmic time, and of the competition between

heating and cooling which finally resurrect star formation and fueling onto SMBHs. The early frequent activities of forming stars and feeding SMBHs result in the substantial increase in stellar mass and SMBH mass within the first two Gyrs as recycled gas from stars is used to form new stars in the central dense regions.

The dominance of SMBH growth over star formation changes over time, depending on how quickly feedback from the accreting mass affects the ambient interstellar medium (ISM) around the SMBH. For example, we investigate the evolution of  $\dot{M}_{\text{BH}}$  and  $\dot{M}_*$  in detail around 3.23 and 13.31 Gyr in Run 6. As shown in Figure 2, the peaks of  $\dot{M}_{\text{BH}}$  in the early accretion phase exceed the Eddington accretion rate for some short period of time. This high accretion onto the SMBH finally produces a strong feedback effect which suppresses the star formation rate. The late SMBH accretion rate, however, is much lower than the Eddington accretion rate even in the peak phase, while  $\dot{M}_*$  rises to  $10^3 M_\odot/\text{yr}$  for a moment. The ratio of  $\dot{M}_*$  to  $\dot{M}_{\text{BH}}$  in this late accretion is consistent with the observed ranges of low-redshift quasars as shown in Figure 2 (e.g. Shi et al. 2009). In the late accretion, the ratio of  $\dot{M}_*$  over  $\dot{M}_{\text{BH}}$  ranges from about 10 to 300 for most time when  $\dot{M}_{\text{BH}} > 1 M_\odot/\text{yr}$ . This range is consistent with the observed range even though the observed range might be limited by samples of quasars. Further discussion of this feature will be given in the next section.

As shown in Figure 3, the mass of the hot, X-ray emitting gas in a galaxy does not change as much as the increase of the newly formed stellar mass or SMBH mass. We measure the total amount of the hot ISM within  $10R_e$  in all models except for Run 1 (where  $R_t$  is smaller than  $10R_e$ ). The mass of outflowed gas is also measured at  $10R_e$ . In the case of Run 1, these two quantities are instead measured at  $R_t$ . In general, stronger evolution is found in models with a small truncation radius. This has important consequences: for example, in Run 1 and 2, the decrease in gas mass is so substantial that intensive star formation and SMBH accretion does not resume, even though heating by stellar and AGN feedback effects is not comparable to that in Run 9 and 10.

Importantly, the total amount of outflowing gas depends only weakly on the truncation radius (see Figure 3). Despite the small  $R_t$ , in Run 1 and 2 the total amount of the gas blown out is not higher than those of other runs because they have less frequent intensive star formation and SMBH accretion events which dump out energy and momentum to produce outflows. We examine this feature further in §3.3.

Figure 4 represents the change of the mass budget as a function of  $R_t$  at 4, 8, and 14 Gyr. The difference of the stellar mass appears at 4 Gyr, while other masses deviate less from each other. But as galaxies evolve, galaxies with smaller  $R_t$  lack more X-ray emitting gas and stellar mass. It is naively true that the smaller galaxies have a smaller amount of gas and stellar mass because of their smaller  $R_t$ . But this trend is not very effective for the



growth of SMBHs as we see in Figure 4, resulting in dispersions of the ratio between stellar mass and SMBH mass.  $M_{BH}/M_*$  in Run 1 is about two times smaller than that in Run 10.

### 3.2. AGN activity and feedback

The frequency of AGN activity varies systematically with  $R_t$  as shown in Figure 1. Smaller  $R_t$  results less frequently in strong SMBH accretion events. Particularly, this change is significant for Runs 1 to 3. For example, Run 1 stops any further intensive accretion after 4 Gyr as shown in Figure 5. Only early peaks of the SMBH optical luminosity are higher than the 10% of the Eddington luminosity. However, Run 6 continues to show AGN activity until 14 Gyr, while the late optical emission from the central SMBH is much lower than the 10% of the Eddington luminosity as in Run 1 (see Figure 5). In other runs such as Run 6 except Runs 1, 2, and 3, this late continuous AGN activity smooths out the dependence of AGN activity on  $R_t$ , and instead shows highly time-dependent stochastic effects. Remarkably, as we see in our simulations, recent observations show a general decrease in the ratio between the SMBH accretion rate and the Eddington rate as the redshift decreases (e.g. Kollmeier et al. 2006; Ballo et al. 2007). In sum, AGN activity in satellite galaxies is expected to decrease with decreasing redshift much more than that of central galaxies.

We note that the late SMBH accretion can reach the limit of the Eddington accretion rate in models with only mechanical feedback effects (see Paper I and II). But in the current models with both radiative and mechanical feedback, the radiative pressure contribution due to dust opacity makes the late peaks of the accretion rate much lower than the Eddington rate (Ciotti & Ostriker 2007) in agreement with recent measurements of the accretion rate and hydrogen column density (Fabian et al. 2009). By 3.5 Gyr mass loss from the initial bulge accumulates an amount of cold gas which can be strongly affected by radiative feedback effects. Therefore, after about 3.5 Gyr all models do not have super-Eddington accretion phases as shown in Figure 1.

Strong AGN activity is generally correlated with the increase in X-ray luminosity from the hot ISM. Despite the differences in  $R_t$  and the consequential difference in AGN activity, the response of the X-ray luminosity to the AGN activity is similar in Runs 2 and 6 as shown in Figure 5. As the SMBH accretion rate increases, the oscillatory response of the hot ISM to AGN feedback begins to produce an oscillation of the X-ray luminosity. When the optical luminosity from the SMBH accretion temporally drops because of extinction, the X-ray luminosity quickly increases (see Pellegrini et al. 2009, for a discussion on the evolution of the nuclear X-ray emission).

The effects from AGN feedback can also be found in the radial distribution of gas temperature and density. Figure 6 shows the two cases of Run 1 and 6 at 3 and 14 Gyr. As we found in Figure 5, both models are in an active phase at 3 Gyr. Basically, the active phase in both models causes the increase in the central temperature. In addition, the consecutive active phases leave the wiggle structure in both temperature and density distribution as the AGN feedback effects propagate to the outer regions on a sound-crossing time scale. At 14 Gyr, Run 1 is in the quite stationary, hot accretion phase, while Run 6 experienced a recent violent nuclear burst within 1 Gyr (see Figure 5). Considering uncertainties of deprojection and radial binning effects in observation, the radial temperature and density distribution of Run 1 is within the observed range of local quiescent elliptical galaxies (see Fukazawa et al. 2006; Humphrey et al. 2006, for examples of observation), although its X-ray luminosity from the hot gas is lower than the observed range of luminosities for the same stellar mass. For example, the central density of the hot ISM is around  $10^{-24}$  to  $10^{-25}(\text{gcm}^{-3})$  in all runs. But the recent AGN activity makes Run 6 have a more disturbed radial structure than Run 1. Moreover, we find a significant difference in the central density between the two runs at 14 Gyr.

Finally, the episodic and net quasar lifetime is measured in all runs, defining the quasar phase with the optical luminosity from the SMBH in  $B$ -band  $M_B < -23$  mag (in Vega magnitude) (e.g., Martini 2004) by using the typical spectral energy distribution of quasar in  $B$ -band (Elvis et al. 1994). This magnitude cut corresponds to about  $L_{\text{BH}} \sim 5 \times 10^{45} \text{erg s}^{-1}$  with the median spectral energy distribution of quasars (Elvis et al. 1994). We define the quasar phase with this  $L_{\text{BH}}$  cut and effective bolometric luminosity from simulations. The effective bolometric luminosity represents bolometric luminosity from AGN with extinction by ISM as explained in Paper I. The episodic lifetime of quasar phase is an interval measured from the increase of the SMBH optical luminosity above  $M_B < -23$  to the drop below this level, while the net quasar lifetime is the sum of these episodic lifetimes. Therefore, each peak of  $\dot{M}_{\text{BH}}$  has its episodic lifetime when it is above  $M_B < -23$ . In Figure 7, we present results for Runs 1, 4, 6, and 9. The episodic lifetime of each quasar phase varies significantly among the peaks of the SMBH accretion. In particular, an extremely short episodic quasar phase is found between long episodic bursts after about 3.5 Gyr. The episodic quasar lifetime ranges from about 0.1 Myr up to about 10 Myr. Even though the simulations with the large  $R_t$  do not experience late luminous quasar phases within the last 2 Gyr (see Figure 1), the net lifetime of quasar phase generally increases as the  $R_t$  increases. But, because the net lifetime in models do not include any possible active phase before 2 Gyr, i.e. the starting epoch of our models, a direct comparison of this net lifetime to observational constraints is not straightforward.

### 3.3. Outflowing gas

Even though the boundary condition of our simulation might not be realistic in detail, it is useful to know the properties of outflowing gas. Probably, the gas blown out of the truncation radius of satellite galaxies will be mixed into the intergalactic medium although the gas will change its temperature and density after mixing with the intergalactic medium. As explained in §3.1, the outflowing mass is measured at  $R_t$  for Run 1, while in other runs the mass flowed out at  $10R_e$ , i.e. 69 kpc, is measured as the outflowing mass. As shown in Figure 3, the total amount of outflowing gas does not show a significant difference between the case of satellites and central galaxies, while the growth of stellar mass is quite low in Runs 1 and 2. Because models with a large  $R_t$  do not lose much gas, the outflowing mass measured at  $10R_e$  represents the pollution of the central gas to outer regions where satellite galaxies can also contribute gas by stripping processes. Therefore, galaxies with a small  $R_t$  are more efficient for enriching the intergalactic medium per galaxy.

Figure 8 illustrates how the high radial velocity and density of gas in models affects the total mass of outflowed gas. The galaxy with the smallest  $R_t$  (Run 1) has expelled high-velocity dense gas continuously. Therefore, despite its smaller outflowing surface area at  $R_t = 51.4$  kpc than other runs, its total mass of outflowed gas is substantial and comparable to the mass measured at  $10R_e$  in other runs. For example, the outflowing velocity for  $R_t = 51.4$  kpc (Run 1) is close to 400 km/s at 4 Gyr. At 14 Gyr, simulations from Run 3 to 10 produce the low-velocity outflow which is slower than 100 km/s. But the difference in density becomes small at late time such as at 14 Gyr, as we also found in Figure 6.

### 3.4. Color of galaxies

Color is one of the well observed properties of elliptical galaxies which are dominated by old stellar populations in the local universe. The simple old stellar population of elliptical galaxies implies that their star formation histories have been significantly quiet although a small amount of recent star formation is possible (e.g. Lucero & Young 2007; Young et al. 2009). But environmental effects such as ram-pressure stripping are expected to make the color of satellite galaxies redder (e.g. Martínez et al. 2008; Weinmann et al. 2009).

In order to investigate the spectral properties of our galaxy models, we construct a color-magnitude diagram of model galaxies by synthesizing spectra based on the star formation history of the simulations. Assuming solar metallicity or half solar metallicity for all stellar populations, the spectra are synthesized by using the BC03 model (Bruzual & Charlot 2003), and the corresponding magnitudes are estimated from the spectra with the SDSS filter bands

(Fukugita et al. 1996). Because we do not consider the complicated metallicity distribution of stellar populations and dust extinction, the derived color cannot be directly compared with the observed colors of elliptical galaxies in various environments. Moreover, because colors of old stellar populations found in ellipticals are strongly affected by age effects with age - metallicity degeneracy (see Renzini 2006, for a review), a direct comparison between our simulations with observed ellipticals need the careful consideration of age and metallicity distributions. Here, we just focus on how different star formation histories in different environments affect the color of galaxies in all runs. For the initial stellar mass at the beginning of simulations, we assumed that the same star formation history before 2 Gyr is described by

$$\dot{M}_* \propto (t/\tau^2) e^{(-t/\tau)}, \quad (6)$$

where  $t$  is a cosmic time and  $\tau = 1$  Gyr (e.g., Nagamine et al. 2006). Therefore, the peak of the initial starburst is at  $t = \tau$ .

In Figure 9, we present the distribution of model galaxies in the SDSS ( $u-r$ ) rest-frame color and  $r$ -band absolute magnitude in AB magnitude at 8.5 and 14 Gyr. All galaxies are brighter and bluer at 8.5 Gyr than at 14 Gyr because most of the stellar mass is dominated by the initial old stellar population which changes its color by passive evolution. But there is a significant variation of the color for simulations with different truncation radii. For instance, Runs 8 and 9 at 8.5 Gyr show bluer color than other models, while becoming green galaxies temporally. At 14 Gyr, the color of the galaxy in Run 6 deviates strongly from those of other runs toward green color because of the recent star formation (see Figure 1). This temporary transition to green color with the increase in stellar mass can be a reason why moderate-luminosity AGN, i.e. a low-accretion AGN, are often found with a green color in the color-magnitude diagram (Hasinger 2008; Schawinski et al. 2009).

In addition to the stellar flux, the color of galaxies can also be affected by AGN radiation if the latter is comparable or more luminous than the radiation from the host galaxy. To study this problem, we add the typical spectral energy distribution of type-I luminous quasars (Vanden Berk et al. 2001) to the synthesized stellar spectra of model galaxies. The quasar spectrum is scaled to the extinction-corrected optical luminosity from simulations, which correspond to the observed luminosity of quasars, before it is added. Because the quasar radiation is substantially bluer than the stellar radiation of quasar hosts, the addition of quasar radiation makes the global color of simulated galaxies bluer, as we show in Figure 10. Particularly, Run 9 is strongly affected by its quasar radiation. The almost coincident activity of star formation with SMBH accretion as shown in Figures 1 and 2, results in the shift of galaxy colors to the blue by radiation from young stars as well as that from quasar phase. Importantly, as observed in AGN host galaxies (e.g Cid Fernandes et al. 2001; Ammons et al. 2009; Silverman et al. 2009), the existence of blue young stellar populations

is related to the strength of the SMBH accretion in our simulations. Therefore, Run 6 has the most significantly different color compared to other runs.

#### 4. Discussion and conclusions

In this paper, we have investigated the effects of AGN feedback (in the form of combined radiative and mechanical energy and momentum deposition) on galaxies in different environments corresponding satellite and central galaxies.

Although not including fully realistic stripping effects, our simulations predict various observable features that can be compared to the current and future observations, and which should change in a systematic way between central and satellite galaxies. The simulation results need to be interpreted as a guide to understand a general consequence of environmental effects. Here, we discuss implications from our simulations.

First of all, the local scaling relationship such as the mass ratio between the SMBH and its host galaxy can have a dispersion due to environmental effects. For example, if gas in a galaxy has experienced stripping, the growth of its SMBH is less disturbed than star formation which generally happens over the whole galaxy. Hence, the mass ratio between the SMBH and the host galaxy of fixed galaxy mass could be significantly higher in satellite ellipticals in galaxy clusters. This also implies that a bias effect on deriving the scaling relationship probably exists due to selecting satellite galaxies less likely as observation samples. Objects measured for their SMBH mass are generally bright objects which might not include galaxies having experienced gas stripping. Even though the recent measurements of the SMBH mass might have an intrinsic scatter of the ratio (e.g. Kim et al. 2008b; Gültekin et al. 2009), the current measurements of the SMBH mass in satellite elliptical galaxies have not been conducted systematically. Probably, the systematic investigation of early-type galaxies in the Virgo Cluster might be useful to test our results for satellites in future (Côté et al. 2006; Decarli et al. 2007; Gallo et al. 2008). But we warn that the uncertainty and biases in measuring the SMBH mass might dominate the dispersions in the mass ratios even for galaxies in the Virgo cluster (e.g. Bernardi et al. 2007).

The results of our simulations also imply the less frequent and earlier termination of AGN activity in satellite galaxies compared to central galaxies (i.e. galaxies with a large  $R_t$ ). This result can be tested against the AGN fraction in galaxy clusters and groups (e.g. Gilmour et al. 2007). The observed AGN fraction in galaxy clusters is generally higher than in field galaxies partially because of the high number density of galaxies (i.e. the effect from the cluster richness) and how AGN activities are selected in radio, X-ray, and IR observations

(e.g. Hickox et al. 2009). When considering this effect of the high number density of galaxies, AGN activity actually seems suppressed in galaxy clusters (e.g. Koulouridis & Plionis 2010). The evolution of AGN fractions in galaxy clusters as a function of redshift also shows the increase in AGN activity at higher redshifts when satellite galaxies are still frequently active in their SMBH accretion, supporting our hypothesis of environmental effects on AGN activity (Galametz et al. 2009; Martini et al. 2009). The frequent multiple intensive SMBH accretion events in simulated central galaxies is consistent with several distinctive observable features of cluster central galaxies. For example, many central galaxies show multiple outburst structures such as several gas clumps and surrounding ripples even though the origin of those observed structures and what kind of AGN activity causes those is still uncertain (e.g. Fabian et al. 2005; Graham et al. 2008; Blanton et al. 2009; Clarke et al. 2009).

The very weak dependence of the ejected mass on  $R_t$  implies that satellite galaxies can be important sources of metal enrichment in the intracluster medium. Even though our simulation does not follow the evolution of the metal contents in the outflowing gas, the mass stripped out of the galaxy, which is about  $2 \times 10^{10} M_\odot$  (see Figure 4), must be metal-rich being produced by gas recycling from the evolving stars and supernovae explosion. As explained in §2, our models are similar to the *leaky box model* of galactic chemical evolution for satellites (Pagel 2009) because of the outflowing boundary condition. Finally, the outflows from both satellites and central galaxies might cause mixing which is coupled to AGN activity and turbulence within the intracluster medium (e.g. O’Sullivan et al. 2005). The detailed abundance patterns in the cluster gas should thus reflect the outflow from the satellite cluster ellipticals in addition to the processes by a cluster central galaxy (Domainko et al. 2006; Schindler & Diaferio 2008; Rasmussen & Ponman 2009; Sivanandam et al. 2009).

The recent star formation in cluster central galaxies (e.g. Rafferty et al. 2008; Kirkpatrick et al. 2009) is also naturally explained in our simulations by continuous recurrence of cooling flows and consequently heating by AGN feedback in galaxies with a large  $R_t$ . In our simulations, star formation from a cooling flow is temporally permitted while some amount of the cooling flow is accreted onto the SMBH and triggers AGN feedback which finally heats up and reverses the cooling flow as the cool gas is consumed by star formation. Contrary to a classical solution to the cooling flow problem in the cluster galaxies which stops the cooling flow completely (see Fabian 1994, for a review), our solution to the cooling flow problem for the cluster central galaxies is simply permitting temporary rejuvenation of star formation and AGN activity which is self-regulated, leading to the termination of the cooling flow (see Ciotti & Ostriker 2007, for a further discussion). This kind of solution can be called the *intermittent cooling flow* scenario (Salomé et al. 2006; Bildfell et al. 2008; Pipino et al. 2009; Wilman et al. 2009). A further test of our results will be the Eddington ratio of the rejuvenated SMBH accretion in local cluster central galaxies because the SMBH accretion

rate in the simulated central galaxies is significantly lower than the Eddington accretion rate despite the change of  $R_t$ .

To make our simulations more realistic, we need to improve our simulations by including two important physics: feedback by a radio jet from AGN activity and cosmological setup of environmental effects. In addition to the limits of our simulations already mentioned in our previous Paper II, for example, 1D calculations, and possible different initial conditions such as models presented in Appendix, the radio jet is an important feedback component for cluster central galaxies in environments of galaxy clusters and groups (Begelman 2004; Königl 2006). The observation of radio jets proves that the kinetic energy of jets is enough to be an effective feedback mode even though we do not have a clear explanation about how much of the relevant energy is transported to ISM and intracluster medium (McNamara & Nulsen 2007; Shin et al. 2011). We note that powerful narrow jets such as that seen in the giant elliptical M87 tend to drill through the ambient gas in the galaxy depositing some amount of energy with a relativistic fluid directly to the intergalactic medium (Ferrari 1998; Owen et al. 2000). Our implementation of stripping effect from different environments is simply parametrized by  $R_t$  in one dimension, and is not close to dynamically changing environmental effects in cosmological evolution (e.g. Takeda et al. 1984; Vollmer et al. 2001; Toniazzo & Schindler 2001). Moreover, our simulations do not include effects from tidal gravitational field which is commonly expected in cluster or group environments (D’Ercole et al. 2000). Although the simple implementation makes the interpretation of simulation results obvious, the direct test of simulations will require better but complicated models of ram-pressure stripping and other environmental processes such as tidal stripping in galaxies which have realistic orbits in galaxy clusters and groups.

### A. Models with lower and higher velocity dispersions

We also examine models with lower and higher initial stellar velocity dispersions of model galaxies than the fiducial model given in the main text. These models correspond to lower and higher ratio of stellar mass over SMBH mass compared with the observed ratio in the local universe (Ciotti et al. 2009a; Shin et al. 2010; Ciotti et al. 2010). Here, we summarize results of the models Run 2, 4, 6, 8, and 10 with the lower velocity dispersion 240 km/s and higher velocity dispersion 280 km/s than the fiducial velocity dispersion 260 km/s.

As shown in Figure 11, the general trend of these models is not different from that of the fiducial model. One of the main differences is the frequency of the active SMBH accretion and star formation phase. As expected, models with the lower initial velocity dispersion

experience the less number of active phases than the others because of a less amount of stellar mass, which supplies materials for SMBH accretion and star formation. The second important feature is a high intensity of star formation rate in the beginning of the models with the higher velocity dispersion, while showing a lower SMBH accretion rate at the same time than the fiducial models. Due to a larger stellar mass in these models, the initial accumulation of cooling gas is large enough to trigger the intensive star formation in the beginning. But this intensive star formation competes with SMBH accretion, resulting in the lower SMBH accretion rate. In the late stage of evolution, the models with the higher velocity dispersion also show higher SMBH and star formation rates than the fiducial models. In particular, the SMBH accretion rate is close to the Eddington accretion rate.

Figure 12 shows that the general patterns found in Figure 4 are still valid with the lower or higher initial stellar velocity dispersion. But the change of ratio between stellar and SMBH masses in the models with the higher velocity dispersion is less dependent of the different truncation radii. This weak sensitivity to the environmental effect is caused by the strong and more late SMBH accretion and the dominating high star formation rate in the models with the higher velocity dispersion.

We are grateful to Michael Strauss, James Gunn, Gillian Knapp, Renyue Cen, Jenny Greene, and Christy Tremonti for useful discussions and careful reading. We thank the anonymous referee for comments which improved this manuscript. We also thank Yong Shi for the data used in Figure 2. M.-S.S. is supported by the Charlotte Elizabeth Procter Fellowship of Princeton University. Computations were performed on the computational facilities of PICSciE (Princeton Institute for Computational Science and Engineering).

## REFERENCES

- Abadi, M. G., Moore, B., & Bower, R. G. 1999, *MNRAS*, 308, 947
- Ammons, S. M., Melbourne, J., Max, C. E., Koo, D. C., & Rosario, D. J. V. 2009, *AJ*, 137, 470
- Ann, H. B., Park, C., & Choi, Y.-Y. 2008, *MNRAS*, 389, 86
- Balogh, M. L., Morris, S. L., Yee, H. K. C., Carlberg, R. G., & Ellingson, E. 1999, *ApJ*, 527, 54
- Ballo, L., et al. 2007, *ApJ*, 667, 97



- Begelman, M. C., & Fabian, A. C. 1990, MNRAS, 244, 26P
- Begelman, M. C. 2004, Coevolution of Black Holes and Galaxies, Cambridge University Press, edited by L. C. Ho, p. 374
- Bernardi, M., Sheth, R. K., Tundo, E., & Hyde, J. B. 2007, ApJ, 660, 267
- Binney, J., & Tabor, G. 1995, MNRAS, 276, 663
- Bildfell, C., Hoekstra, H., Babul, A., & Mahdavi, A. 2008, MNRAS, 389, 1637
- Blanton, E. L., Randall, S. W., Douglass, E. M., Sarazin, C. L., Clarke, T. E., & McNamara, B. R. 2009, ApJ, 697, L95
- Brighenti, F., & Mathews, W. G. 1999, ApJ, 512, 65
- Bruzual, G., & Charlot, S. 2003, MNRAS, 344, 1000
- Cardiel, N., Gorgas, J., & Aragon-Salamanca, A. 1998, MNRAS, 298, 977
- Cid Fernandes, R., Heckman, T., Schmitt, H., Delgado, R. M. G., & Storchi-Bergmann, T. 2001, ApJ, 558, 81
- Ciotti, L., & Ostriker, J. P. 2007, ApJ, 665, 1038
- Ciotti, L., Ostriker, J. P., & Proga, D. 2009a, ApJ, 699, 89 (Paper I)
- Ciotti, L., Ostriker, J. P., & Proga, D. 2010, ApJ, 717, 708 (Paper III)
- Clarke, T. E., Blanton, E. L., Sarazin, C. L., Anderson, L. D., Gopal-Krishna, Douglass, E. M., & Kassim, N. E. 2009, ApJ, 697, 1481
- Côté, P., et al. 2006, ApJS, 165, 57
- Cowie, L. L., & Songaila, A. 1977, Nature, 266, 501
- Decarli, R., Gavazzi, G., Arosio, I., Cortese, L., Boselli, A., Bonfanti, C., & Colpi, M. 2007, MNRAS, 381, 136
- D’Ercole, A., Recchi, S., & Ciotti, L. 2000, ApJ, 533, 799
- Di Matteo, T., Colberg, J., Springel, V., Hernquist, L., & Sijacki, D. 2008, ApJ, 676, 33
- Domainko, W., et al. 2006, A&A, 452, 795
- Elvis, M., et al. 1994, ApJS, 95, 1

- Fabian, A. C. 1994, *ARA&A*, 32, 277
- Fabian, A. C., Sanders, J. S., Taylor, G. B., & Allen, S. W. 2005, *MNRAS*, 360, L20
- Fabian, A. C., Celotti, A., & Erlund, M. C. 2006, *MNRAS*, 373, L16
- Fabian, A. C., Vasudevan, R. V., Mushotzky, R. F., Winter, L. M., & Reynolds, C. S. 2009, *MNRAS*, 394, L89
- Ferrarese, L., & Merritt, D. 2000, *ApJ*, 539, L9
- Ferrarese, L. 2002, *ApJ*, 578, 90
- Ferrari, A. 1998, *ARA&A*, 36, 539
- Fukazawa, Y., Botoya-Nones, J. G., Pu, J., Ohto, A., & Kawano, N. 2006, *ApJ*, 636, 698
- Fukugita, M., Ichikawa, T., Gunn, J. E., Doi, M., Shimasaku, K., & Schneider, D. P. 1996, *AJ*, 111, 1748
- Gabor, J. M., et al. 2009, *ApJ*, 691, 705
- Gaetz, T. J., Salpeter, E. E., & Shaviv, G. 1987, *ApJ*, 316, 530
- Galametz, A., et al. 2009, *ApJ*, 694, 1309
- Gallo, E., Treu, T., Jacob, J., Woo, J.-H., Marshall, P. J., & Antonucci, R. 2008, *ApJ*, 680, 154
- Gebhardt, K., et al. 2000, *ApJ*, 539, L13
- Gilmour, R., Gray, M. E., Almaini, O., Best, P., Wolf, C., Meisenheimer, K., Papovich, C., & Bell, E. 2007, *MNRAS*, 380, 1467
- Graham, J., Fabian, A. C., & Sanders, J. S. 2008, *MNRAS*, 391, 1749
- Grogin, N. A., et al. 2005, *ApJ*, 627, L97
- Gültekin, K., et al. 2009, *ApJ*, 698, 198
- Gunn, J. E., & Gott, J. R. I. 1972, *ApJ*, 176, 1
- Håring, N., & Rix, H.-W. 2004, *ApJ*, 604, L89
- Hasinger, G. 2008, *A&A*, 490, 905

- Hester, J. A. 2006, *ApJ*, 647, 910
- Hickox, R. C., et al. 2009, *ApJ*, 696, 891
- Humphrey, P. J., Buote, D. A., Gastaldello, F., Zappacosta, L., Bullock, J. S., Brighenti, F., & Mathews, W. G. 2006, *ApJ*, 646, 899
- Jahnke, K., et al. 2004, *ApJ*, 614, 568
- Johansson, P. H., Naab, T., & Burkert, A. 2009, *ApJ*, 690, 802
- Kapferer, W., Sluka, C., Schindler, S., Ferrari, C., & Ziegler, B. 2009, *A&A*, 499, 87
- Kawata, D., & Mulchaey, J. S. 2008, *ApJ*, 672, L103
- Kim, D.-W., Kim, E., Fabbiano, G., & Trinchieri, G. 2008, *ApJ*, 688, 931
- Kim, M., Ho, L. C., Peng, C. Y., Barth, A. J., Im, M., Martini, P., & Nelson, C. H. 2008, *ApJ*, 687, 767
- Kirkpatrick, C. C., et al. 2009, *ApJ*, 697, 867
- Kollmeier, J. A., et al. 2006, *ApJ*, 648, 128
- Königl, A. 2006, *Memorie della Societa Astronomica Italiana*, 77, 598
- Kormendy, J., & Richstone, D. 1995, *ARA&A*, 33, 581
- Koulouridis, E., & Plionis, M. 2010, preprint, arXiv:1003.0753
- Krongold, Y., Nicastro, F., Elvis, M., Brickhouse, N., Binette, L., Mathur, S., & Jiménez-Bailón, E. 2007, *ApJ*, 659, 1022
- Kurosawa, R., Proga, D., & Nagamine, K. 2009, *ApJ*, 707, 823
- Kurosawa, R., & Proga, D. 2009, *ApJ*, 693, 1929
- Kurosawa, R., & Proga, D. 2009, *MNRAS*, 397, 1791
- Larson, R. B., Tinsley, B. M., & Caldwell, C. N. 1980, *ApJ*, 237, 692
- Letawe, Y., Magain, P., Letawe, G., Courbin, F., & Hutsemékers, D. 2008, *ApJ*, 679, 967
- Li, C., Kauffmann, G., Heckman, T. M., White, S. D. M., & Jing, Y. P. 2008, *MNRAS*, 385, 1915

- Livio, M., Regev, O., & Shaviv, G. 1980, *ApJ*, 240, L83
- Lucero, D. M., & Young, L. M. 2007, *AJ*, 134, 2148
- Magorrian, J., et al. 1998, *AJ*, 115, 2285
- Marconi, A., & Hunt, L. K. 2003, *ApJ*, 589, L21
- Martini, P. 2004, *Coevolution of Black Holes and Galaxies*, 169
- Martini, P., Sivakoff, G. R., & Mulchaey, J. S. 2009, *ApJ*, 701, 66
- Martínez, H. J., Coenda, V., & Muriel, H. 2008, *MNRAS*, 391, 585
- McNamara, B. R., & Nulsen, P. E. J. 2007, *ARA&A*, 45, 117
- McCarthy, I. G., Frenk, C. S., Font, A. S., Lacey, C. G., Bower, R. G., Mitchell, N. L., Balogh, M. L., & Theuns, T. 2008, *MNRAS*, 383, 593
- Merritt, D. 1983, *ApJ*, 264, 24
- Moore, B., Lake, G., Quinn, T., & Stadel, J. 1999, *MNRAS*, 304, 465
- Nagamine, K., Ostriker, J. P., Fukugita, M., & Cen, R. 2006, *ApJ*, 653, 881
- Narayan, R., McClintock, J. E., & Yi, I. 1996, *ApJ*, 457, 821
- Nepveu, M. 1985, *A&A*, 149, 459
- Nulsen, P. E. J. 1982, *MNRAS*, 198, 1007
- O’Dea, C. P., et al. 2008, *ApJ*, 681, 1035
- O’Sullivan, E., Vrtilek, J. M., & Kempner, J. C. 2005, *ApJ*, 624, L77
- Owen, F. N., Eilek, J. A., & Kassim, N. E. 2000, *ApJ*, 543, 611
- Pagel, B. E. J. 2009, *Nucleosynthesis and Chemical Evolution of Galaxies*, 2nd ed., Cambridge University Press
- Pei, Y. C. 1992, *ApJ*, 395, 130
- Pellegrini, S., Ciotti, L., & Ostriker, J. P. 2009, *Advances in Space Research*, 44, 340
- Pipino, A., Kaviraj, S., Bildfell, C., Babul, A., Hoekstra, H., & Silk, J. 2009, *MNRAS*, 395, 462

- Quilis, V., Moore, B., & Bower, R. 2000, *Science*, 288, 1617
- Rafferty, D. A., McNamara, B. R., Nulsen, P. E. J., & Wise, M. W. 2006, *ApJ*, 652, 216
- Rafferty, D. A., McNamara, B. R., & Nulsen, P. E. J. 2008, *ApJ*, 687, 899
- Randall, S., Nulsen, P., Forman, W. R., Jones, C., Machacek, M., Murray, S. S., & Maughan, B. 2008, *ApJ*, 688, 208
- Rasmussen, J., & Ponman, T. J. 2009, *MNRAS*, 399, 239
- Reichard, T. A., Heckman, T. M., Rudnick, G., Brinchmann, J., Kauffmann, G., & Wild, V. 2009, *ApJ*, 691, 1005
- Reiprich, T., Kempner, J., & Soker, N. 2004, *The Riddle of Cooling Flows in Galaxies and Clusters of galaxies*
- Renzini, A. 2006, *ARA&A*, 44, 141
- Roediger, E., & Brüggen, M. 2008, *MNRAS*, 388, L89
- Salomé, P., et al. 2006, *A&A*, 454, 437
- Sánchez, S. F., et al. 2004, *ApJ*, 614, 586
- Sazonov, S. Y., Ostriker, J. P., & Sunyaev, R. A. 2004, *MNRAS*, 347, 144
- Sazonov, S. Y., Ostriker, J. P., Ciotti, L., & Sunyaev, R. A. 2005, *MNRAS*, 358, 168
- Schawinski, K., Virani, S., Simmons, B., Urry, C. M., Treister, E., Kaviraj, S., & Kushkuley, B. 2009, *ApJ*, 692, L19
- Schindler, S., & Diaferio, A. 2008, *Space Science Reviews*, 134, 363
- Shi, Y., Rieke, G. H., Ogle, P., Jiang, L., & Diamond-Stanic, A. M. 2009, *ApJ*, 703, 1107
- Shin, M.-S., Ostriker, J. P., & Ciotti, L. 2010, *ApJ*, 711, 268 (Paper II)
- Shin, M.-S., Strauss, M. A., & Tojeiro, R. 2011, *MNRAS*, 410, 1583
- Silverman, J. D., et al. 2009, *ApJ*, 696, 396
- Sivanandam, S., Zabludoff, A. I., Zaritsky, D., Gonzalez, A. H., & Kelson, D. D. 2009, *ApJ*, 691, 1787

- Smith, R. J., Lucey, J. R., Hudson, M. J., Allanson, S. P., Bridges, T. J., Hornschemeier, A. E., Marzke, R. O., & Miller, N. A. 2009, *MNRAS*, 392, 1265
- Soltan, A. 1982, *MNRAS*, 200, 115
- Spitzer, L. J., & Baade, W. 1951, *ApJ*, 113, 413
- Springel, V., Di Matteo, T., & Hernquist, L. 2005, *ApJ*, 620, L79
- Stevens, I. R., Acreman, D. M., & Ponman, T. J. 1999, *MNRAS*, 310, 663
- Sun, M., Vikhlinin, A., Forman, W., Jones, C., & Murray, S. S. 2005, *ApJ*, 619, 169
- Tabor, G., & Binney, J. 1993, *MNRAS*, 263, 323
- Takeda, H., Nulsen, P. E. J., & Fabian, A. C. 1984, *MNRAS*, 208, 261
- Toniazzo, T., & Schindler, S. 2001, *MNRAS*, 325, 509
- Tonnesen, S., & Bryan, G. L. 2008, *ApJ*, 684, L9
- Tortora, C., Napolitano, N. R., Romanowsky, A. J., Capaccioli, M., & Covone, G. 2009, *MNRAS*, 396, 1132
- Valluri, M., & Jog, C. J. 1990, *ApJ*, 357, 367
- Vanden Berk, D. E., et al. 2001, *AJ*, 122, 549
- van den Bosch, F. C., Aquino, D., Yang, X., Mo, H. J., Pasquali, A., McIntosh, D. H., Weinmann, S. M., & Kang, X. 2008, *MNRAS*, 387, 79
- van Dokkum, P. G., et al. 2010, *ApJ*, 709, 1018
- Veilleux, S., Cecil, G., & Bland-Hawthorn, J. 2005, *ARA&A*, 43, 769
- Vollmer, B., Cayatte, V., Balkowski, C., & Duschl, W. J. 2001, *ApJ*, 561, 708
- Weinmann, S. M., Kauffmann, G., van den Bosch, F. C., Pasquali, A., McIntosh, D. H., Mo, H., Yang, X., & Guo, Y. 2009, *MNRAS*, 394, 1213
- White, D. A., Fabian, A. C., Forman, W., Jones, C., & Stern, C. 1991, *ApJ*, 375, 35
- Wilman, R. J., Edge, A. C., & Swinbank, A. M. 2009, *MNRAS*, 395, 1355
- Young, L. M., Bendo, G. J., & Lucero, D. M. 2009, *AJ*, 137, 3053

Yu, Q., & Tremaine, S. 2002, MNRAS, 335, 965

Table 1: Truncation radius  $R_t$  of the hydrodynamical grid

Run	Radius (kpc)	Run	Radius (kpc)
1	51.4	6	239.7
2	88.5	7	287.3
3	127.2	8	344.4
4	166.9	9	377.0
5	218.9	10	412.8

---

Note. — The effective radius of the galaxy models is 6.9 kpc at the beginning of the simulation.



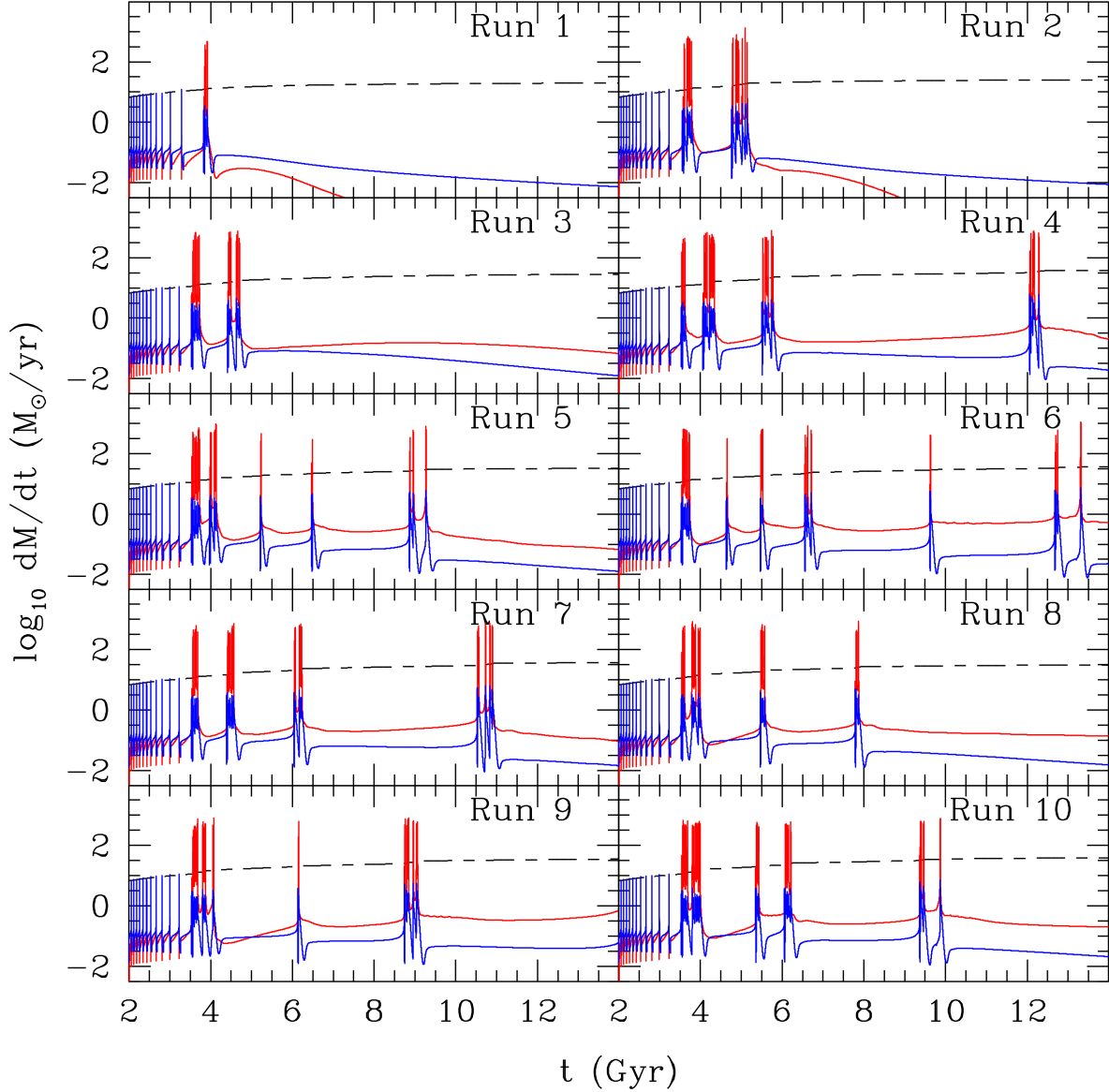


Fig. 1.— SMBH mass accretion rate and star formation rate. The SMBH mass accretion rate  $\dot{M}_{\text{BH}}$  (blue) and star formation rate  $\dot{M}_*$  (red) show a strong time-dependence with multiple intensive events consisting of several peaks.  $\dot{M}_{\text{BH}}$  is usually lower than the Eddington accretion rate (short-long dashed line). Note how the frequency of the peaks of  $\dot{M}_{\text{BH}}$  and  $\dot{M}_*$  depends on the truncation radius, particularly increasing from Run 1 ( $R_t = 51.4$  kpc) to Run 3 ( $R_t = 127.2$  kpc).

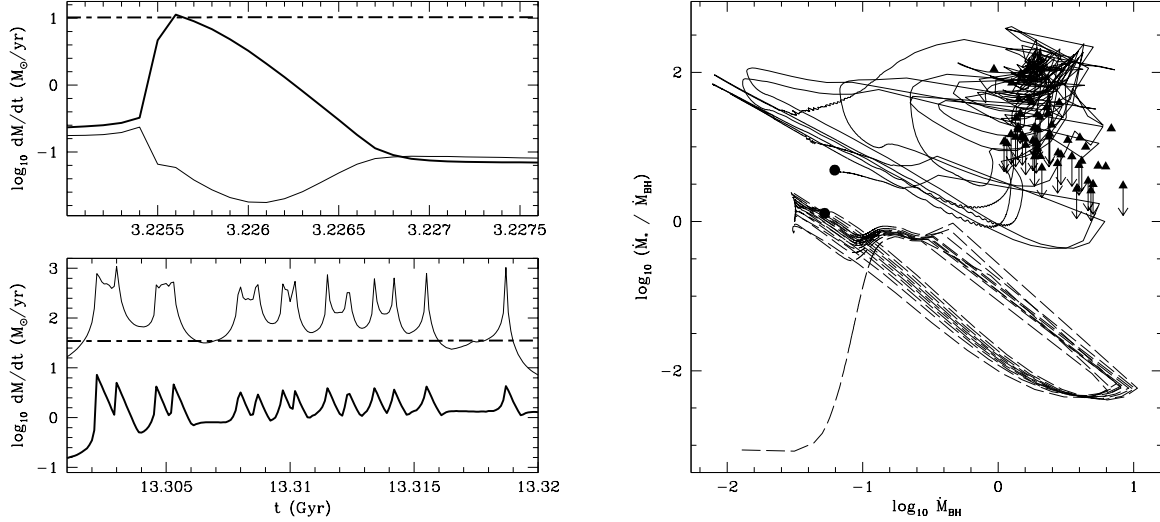


Fig. 2.— Star formation rate ( $\dot{M}_{*}$ ) and SMBH mass accretion rate ( $\dot{M}_{\text{BH}}$ ) around 3.23 Gyr (left top) and 13.31 Gyr (left bottom) and the distribution of  $\dot{M}_{*}/\dot{M}_{\text{BH}}$  with respect to  $\dot{M}_{\text{BH}}$  (right) in Run 6. Only early peaks of  $\dot{M}_{\text{BH}}$  (thick solid line) are higher than the Eddington accretion rate (thick short-long dashed line) as shown in the left top panel. The early SMBH accretion is so strong that the following star formation is suppressed, while the late SMBH accretion is predominated by the concurrent intensive star formation. When  $\dot{M}_{*}$  (thin solid line) is high,  $\dot{M}_{\text{BH}}$  is generally low in the early SMBH accretion as apparent in the left top panel. But when  $\dot{M}_{*}$  is high,  $\dot{M}_{\text{BH}}$  is also high in the late SMBH accretion. The difference between the early SMBH accretion pattern and the late pattern is clearly found in the right panel showing the change for the time earlier than 3 Gyr (dashed line) and later than 7.5 Gyr (solid line). Dots represent 3 and 7.5 Gyr, respectively. Triangles and triangles with arrows represent observed ratios and upper limits from Shi et al. (2009), respectively.

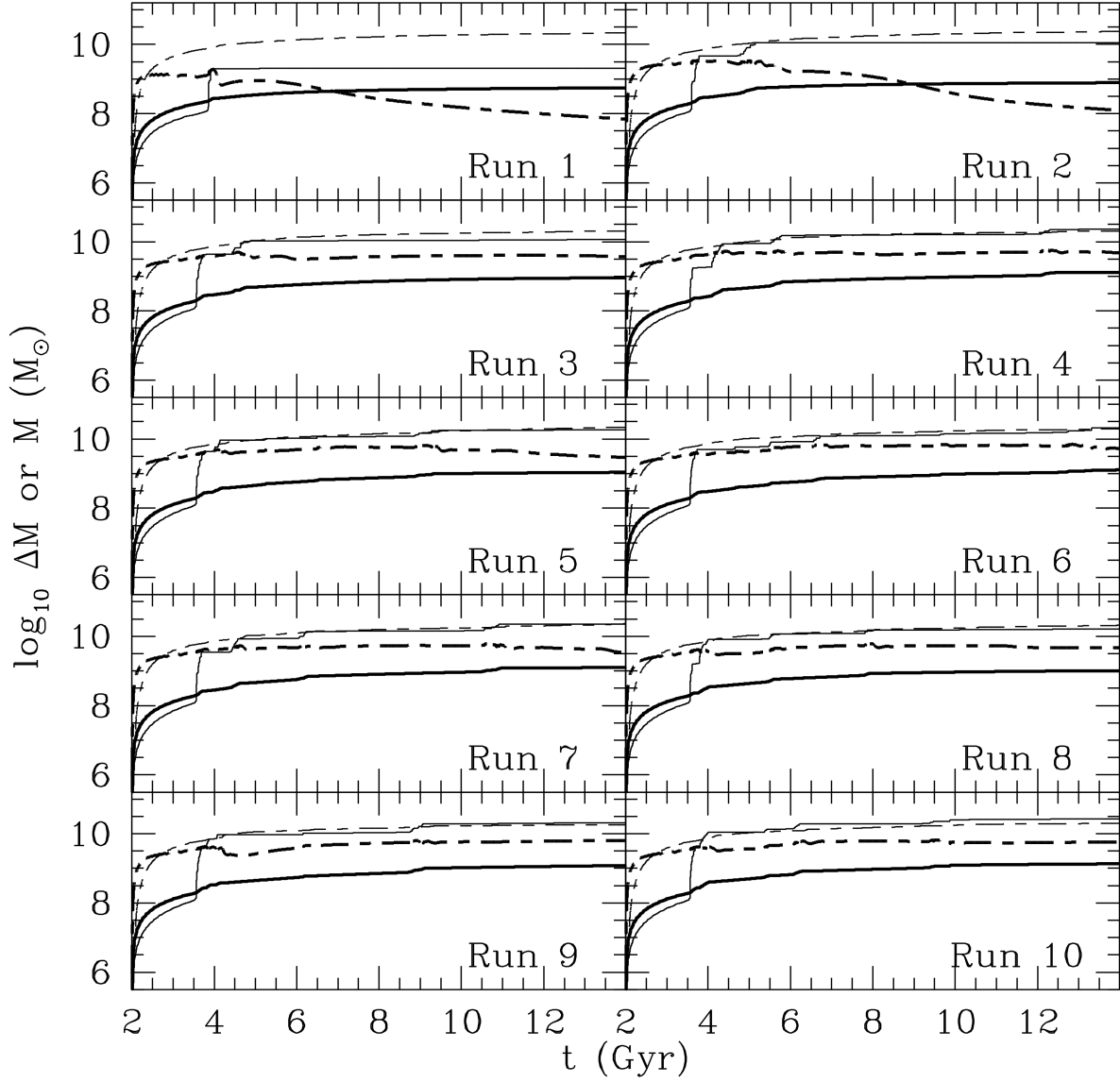


Fig. 3.— Time evolution of mass components in the galaxy models. The different evolution of  $\dot{M}_{\text{BH}}$  and  $\dot{M}_*$  for different values of  $R_t$  results in different final values of the mass ratios between the SMBH and stars, and different amounts of gas that are blown out. The mass  $\Delta M_{\text{BH}}$  added to the SMBH (*thick solid line*) is in general much smaller than the change in the stellar mass,  $\Delta M_*$  (*thin solid line*). The total amount of X-ray emitting hot gas contained in the galaxy (*thick short-long dashed line*) decreases as  $M_{\text{BH}}$ ,  $M_*$ , and the total mass of outflowing gas (*thin short-long dashed line*) increase, particularly in the models with small truncation radii.

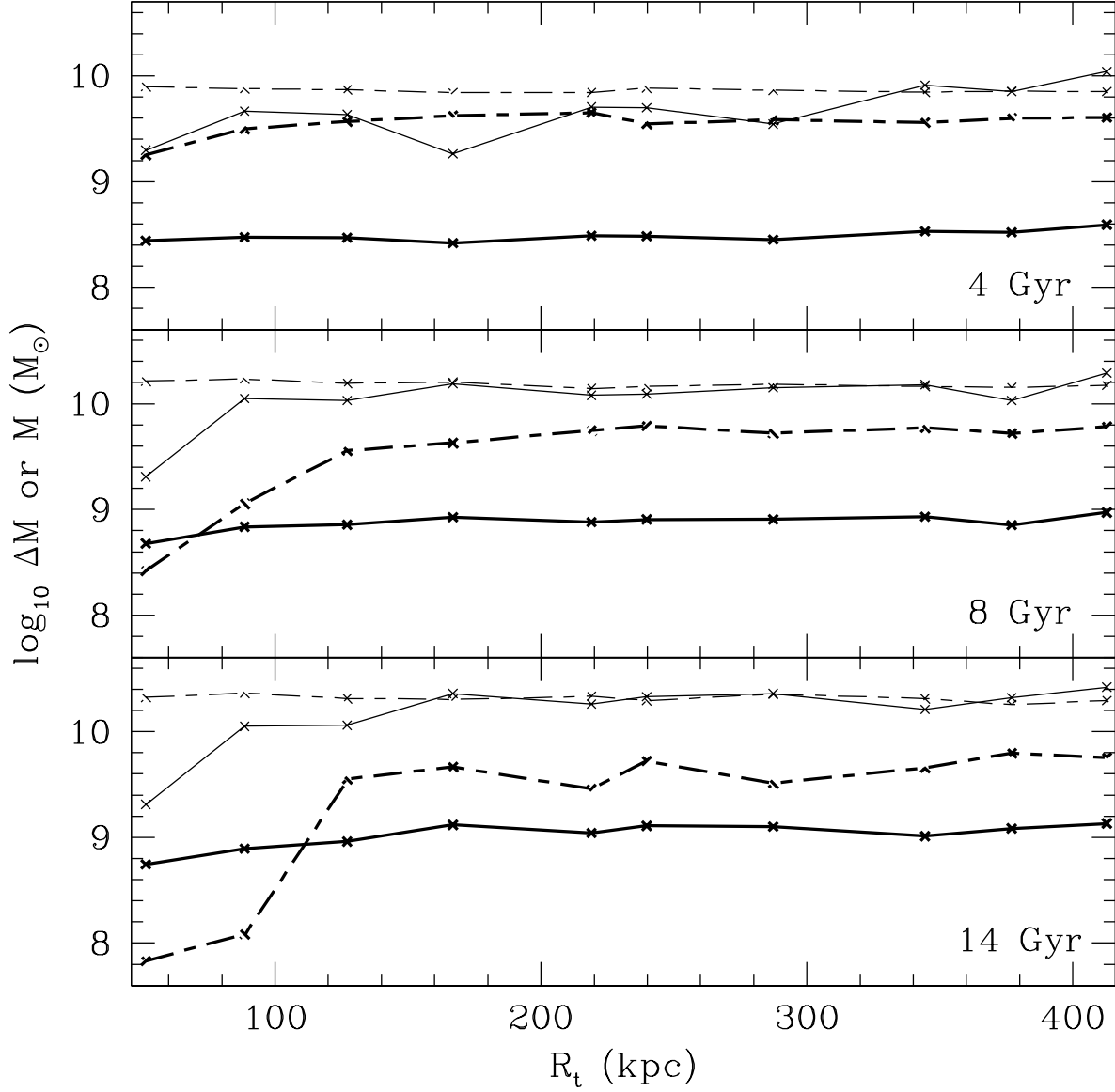


Fig. 4.— Comparison of the mass budget at 4, 8, and 14 Gyr for different values of  $R_t$ . The presentation follows the same line styles as given in Figure 3. At 2 Gyr differences among the simulations are not significant. As effects from different star formation and SMBH accretion history accumulate, the increase in stellar mass and the total mass of gas in Run 1 and 2 begin to deviate from other simulations. But the amount of outflowing gas does not change much with respect to  $R_t$ .

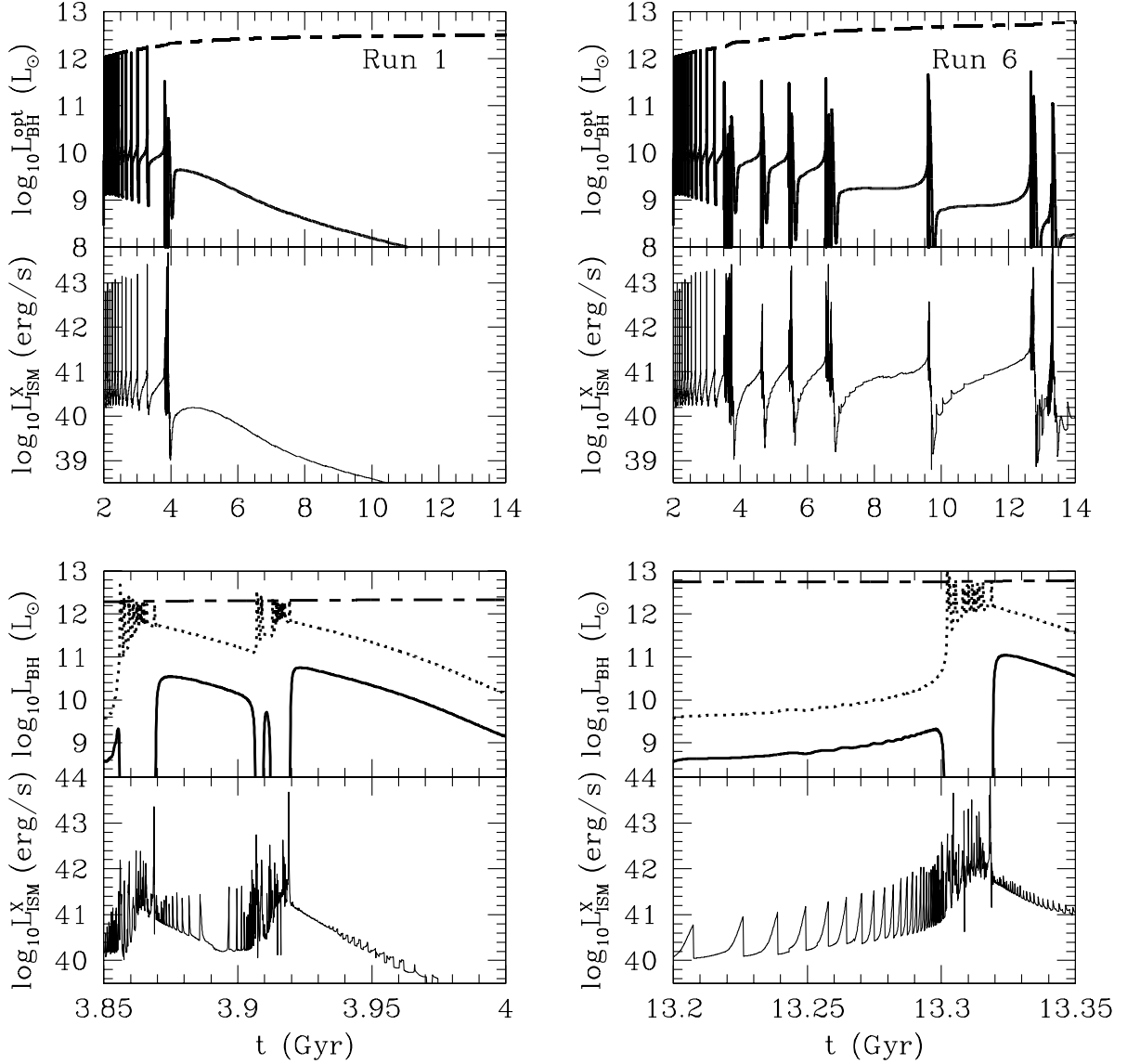


Fig. 5.— Optical luminosity from accretion onto SMBHs and X-ray luminosity from hot ISM in their host galaxies for Run 1 and 6. In both simulations, the optical luminosity of SMBHs  $L_{\text{BH}}^{\text{opt}}$  (*thick solid line*) correlates with the change of X-ray luminosity  $L_{\text{ISM}}^{\text{X}}$  (*thin solid line*). The optical luminosity from the accretion is usually below the 10% of the Eddington luminosity (*short-long dashed line*). We note that the optical luminosity is derived considering the extinction effects (Ciotti & Ostriker 2007). The bottom plots show the complex evolution of Run 1 at about 3.9 Gyr and of Run 6 at about 13.3 Gyr with bolometric luminosity from SMBH without dust extinction (*dotted line*). When  $L_{\text{BH}}^{\text{opt}}$ , i.e. the SMBH accretion rate, is high,  $L_{\text{ISM}}^{\text{X}}$  shows the oscillatory structure because of feedback from the accreting SMBH. Yet, the accumulated cold gas finally strongly extincts optical luminosity from the accreting SMBH while  $L_{\text{ISM}}^{\text{X}}$  and the SMBH bolometric luminosity increase around 3.86, 3.92, and 13.31 Gyr.

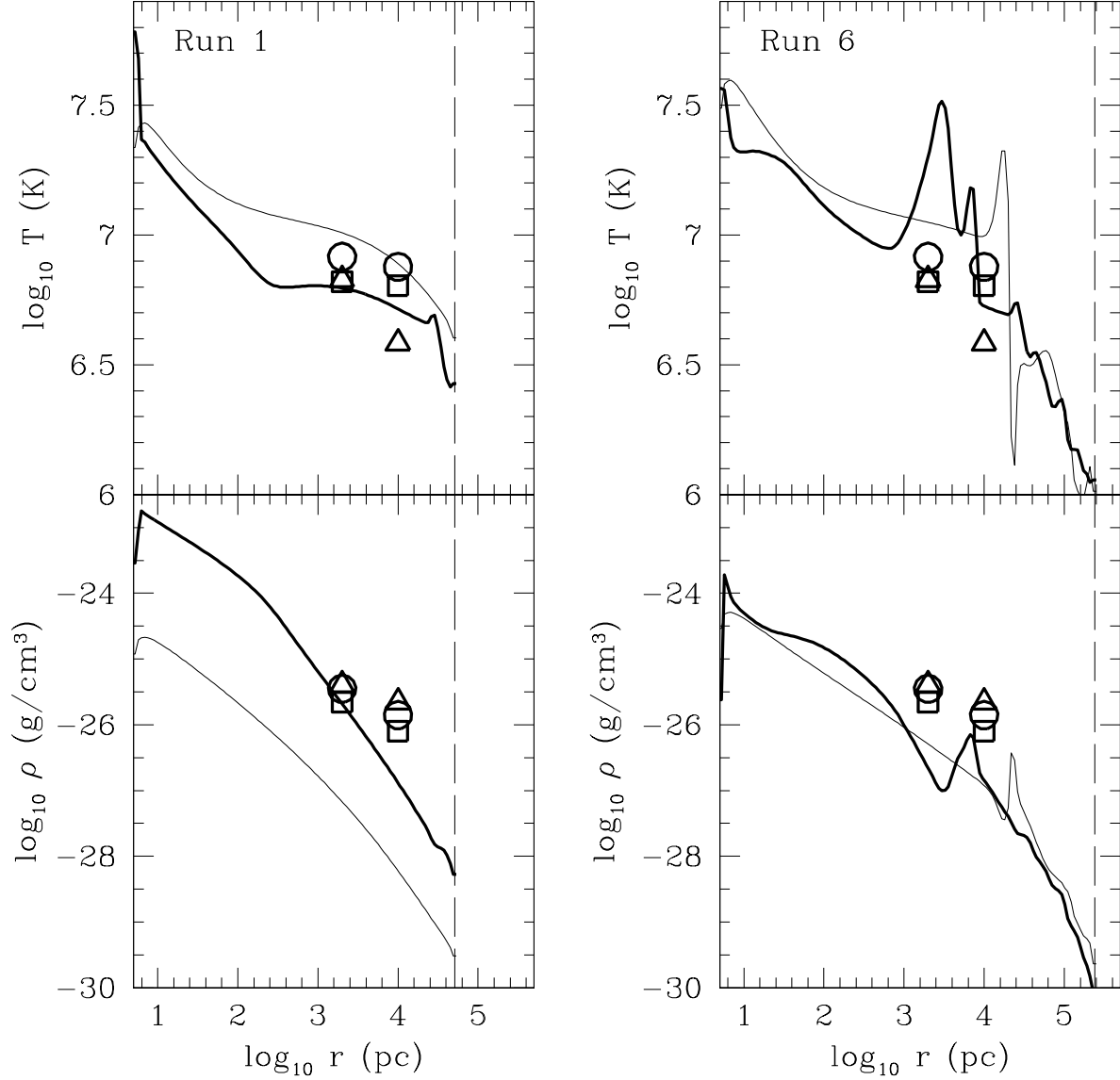


Fig. 6.— Radial distribution of the ISM temperature and density in Run 1 and 6. The truncation radii are indicated as dashed lines. At 14 Gyr (*thin line*), Run 1 and 6 are found in the low-luminosity hot accretion phase; the higher central temperature and density in Run 6 are because of the influence of the larger final SMBH mass. However, Run 6 still shows the effect from its recent active phase forming the sharp shell structure. When both models are in the active phase at 3 Gyr (*thick line*) either increase of core temperature or shell structures appears in the radial distributions. Triangles, squares, and circles correspond to observed values at 2 and 10 kpc in NGC 4125, NGC 720, and NGC 6482, respectively, from Humphrey et al. (2006).

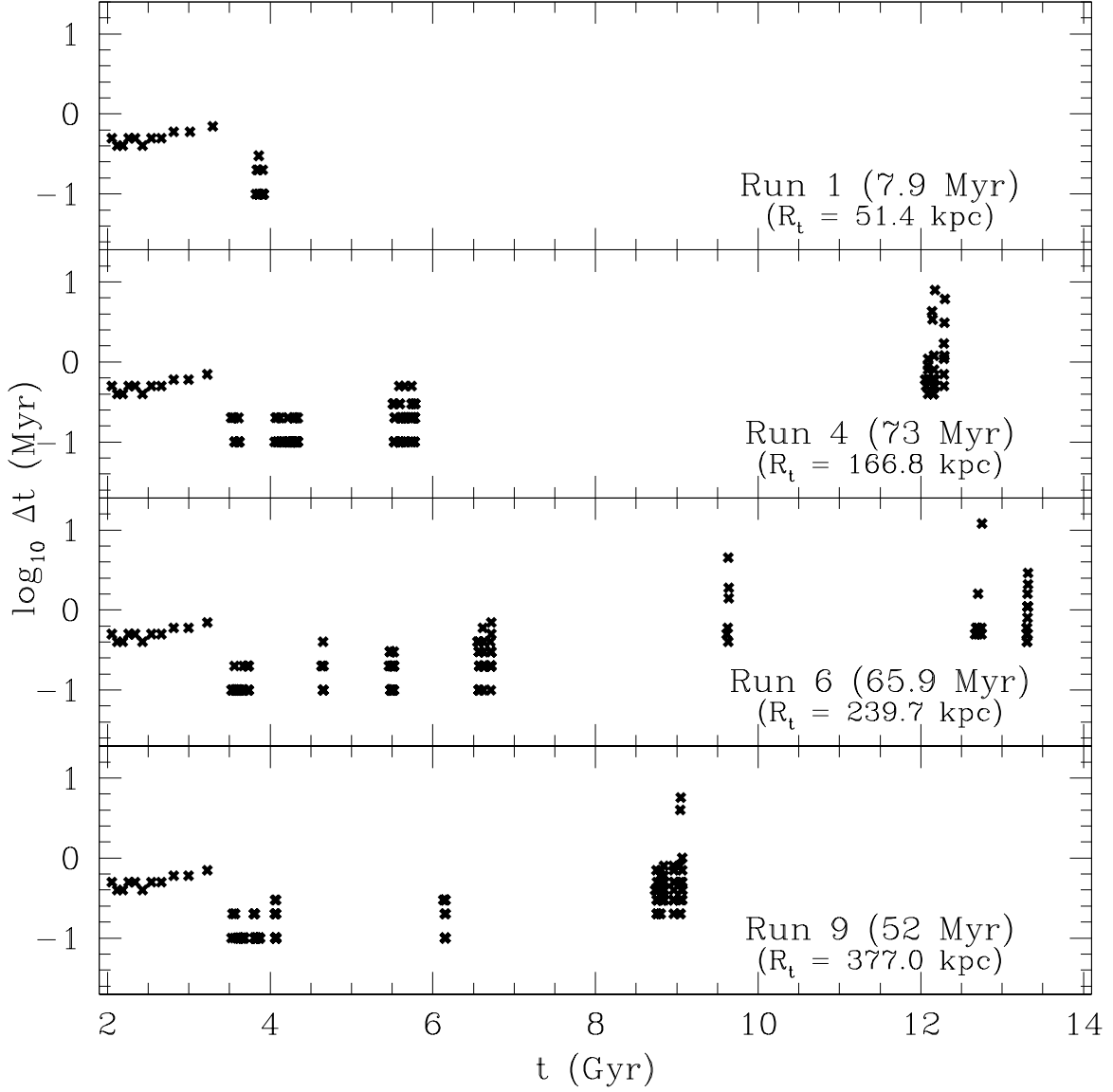


Fig. 7.— Episodic and net lifetime of optically luminous quasar phase (i.e.  $M_B < -23$  mag) in Run 1, 4, 6, and 9. The episodic lifetime is presented for each peak of  $\dot{M}_{\text{BH}}$  as cross symbols. The net lifetime is given in the parenthesis next to the simulation number. The episodic lifetime increases as the simulation continues until about 3.5 Gyr when the peaks of SMBHs accretion rate are higher than the Eddington accretion rate.

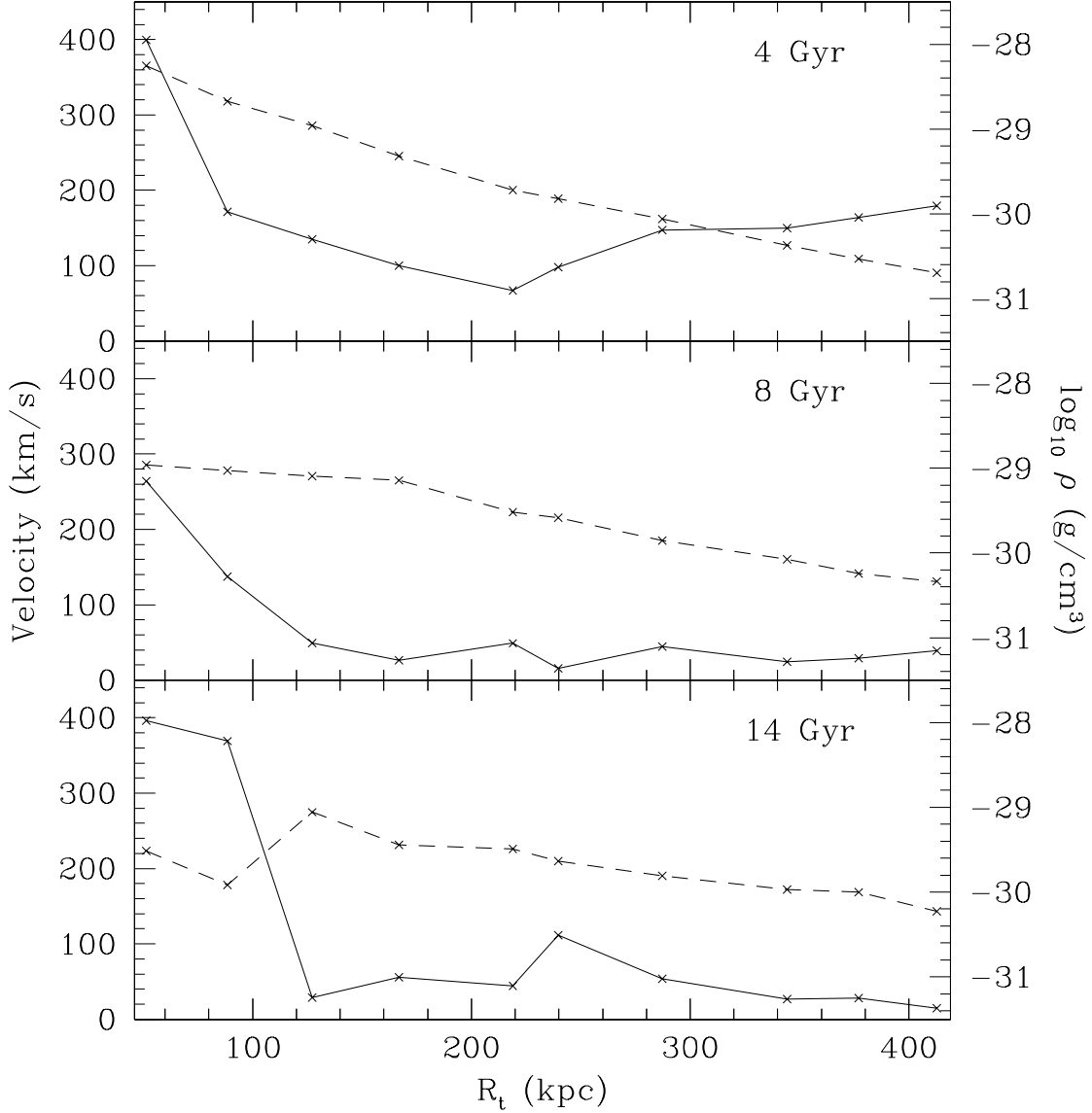


Fig. 8.— Outflow velocity and density as a function of  $R_t$  at 4, 8, and 14 Gyr. Velocity (solid line) and density (dashed line) is estimated on the last radial grid point  $R_t$  which represents the boundary of gas truncation. Models with small  $R_t$  have the more dense and fast flows that pass out the truncation radius, producing the amount of mass loss which is comparable to that of models with the large  $R_t$  when we measure the mass loss at  $10R_e$ . We note that the mass flowing out at late times is negligible for large values of  $R_t$ .



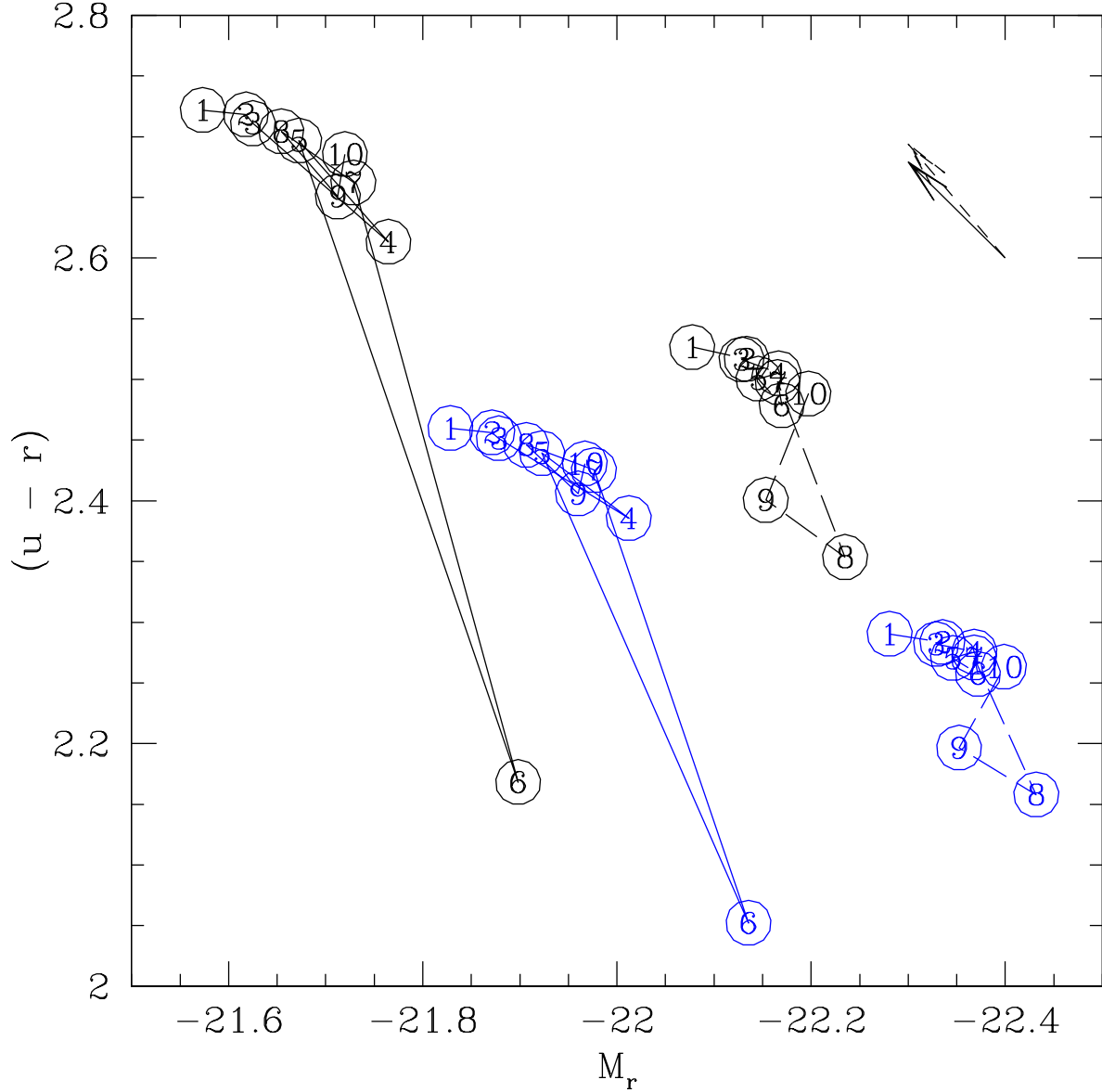


Fig. 9.— Systematic color-magnitude diagram at 8.5 Gyr (*dashed line*) and 14 Gyr (*solid line*) without the optical radiation from the SMBH. From the star formation history of each run, we retrieve the synthesized spectra by using the BC03 model (Bruzual & Charlot 2003). Solar metallicity is assumed for black lines, while half solar metallicity is used for blue lines. The effects from dust extinction are not considered in the construction of spectra. The numbers in circles represent the name of the run. The arrows represents color excess for  $A_r = 0.1$  with the dust extinction curves of the Milky Way (*solid line*) and Small Magellanic Cloud (*dashed line*) from Pei (1992), respectively.

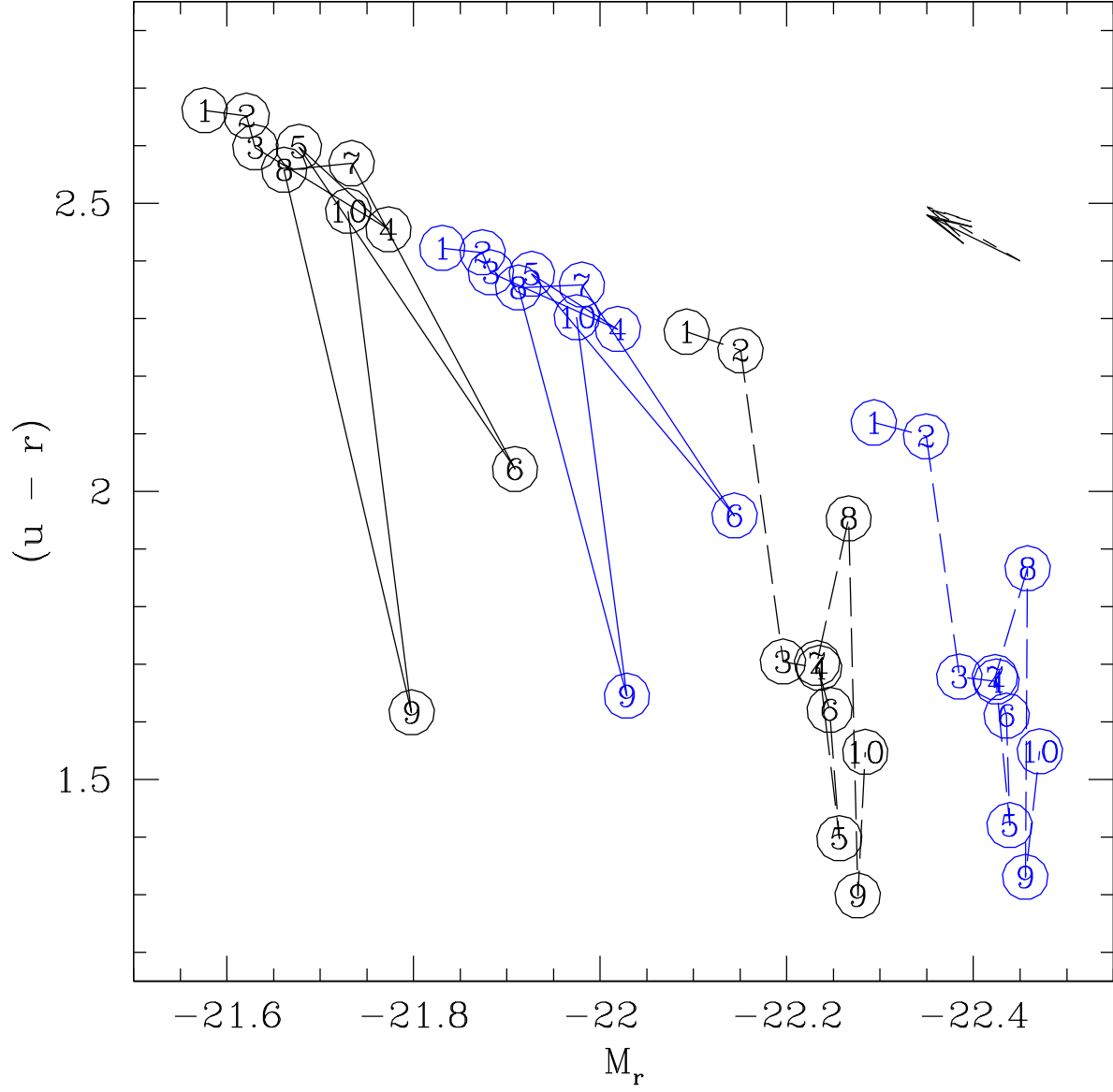


Fig. 10.— Same as Fig. 9, but with the optical radiation from the SMBH. The included quasar spectrum is a luminosity-scaled spectrum of type-I quasar (Vanden Berk et al. 2001).

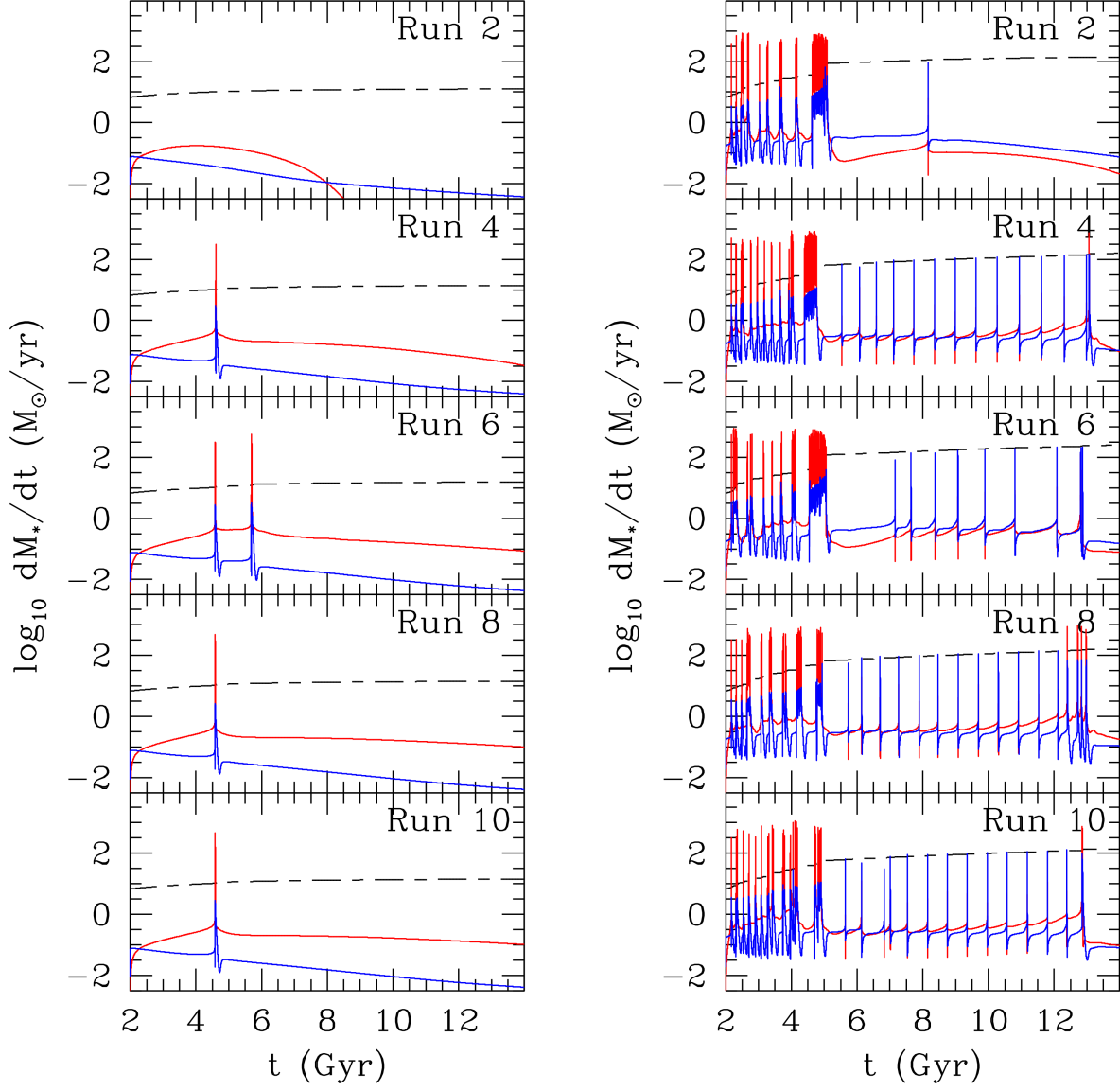


Fig. 11.— Same as Fig. 1, but with the initial velocity dispersions of 240 km/s (*left*) and 280 km/s (*right*) for Runs 2, 4, 6, 8, and 10.

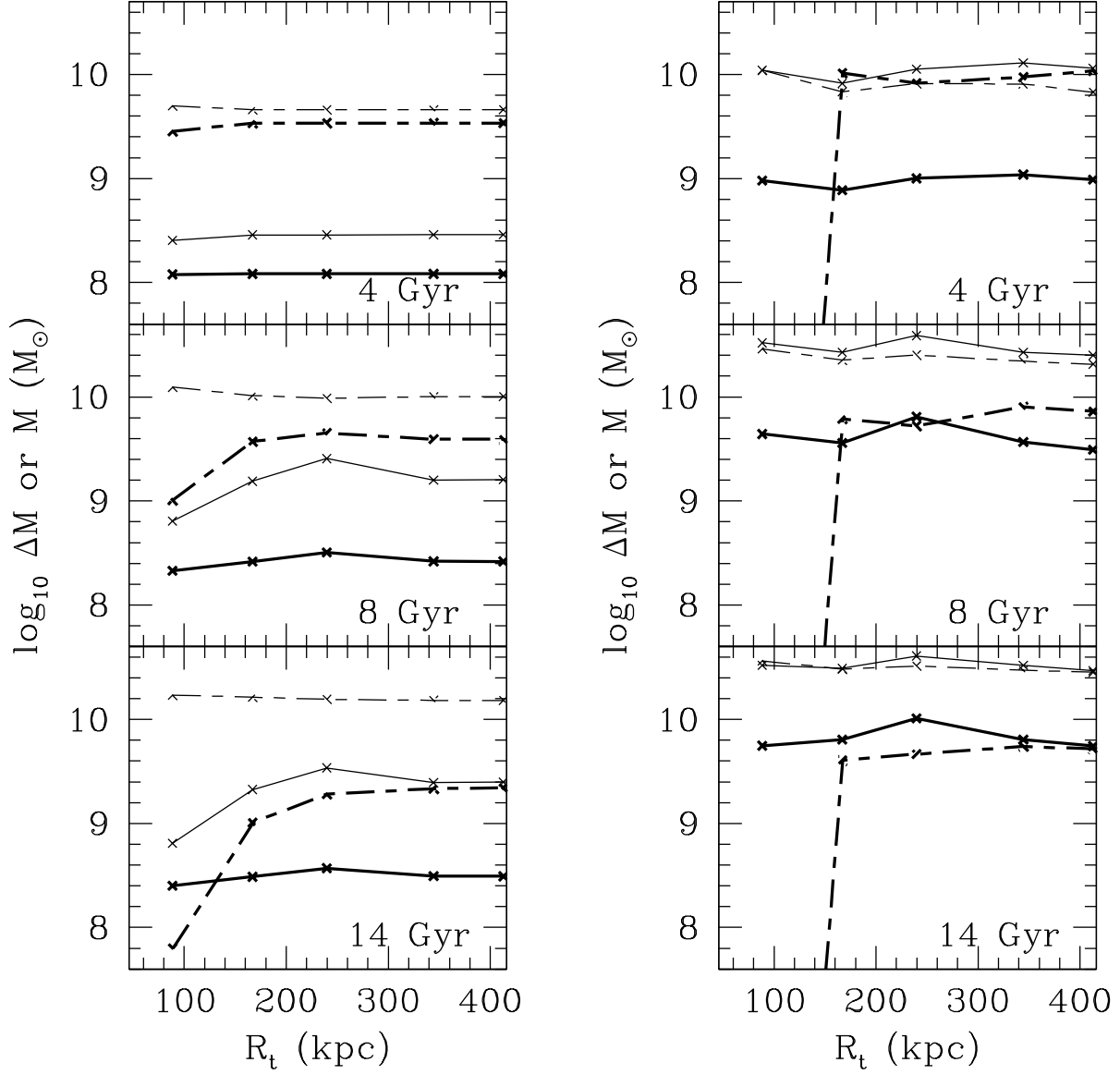


Fig. 12.— Same as Fig. 4, but with the initial velocity dispersions of 240 km/s (*left*) and 280 km/s (*right*) for Runs 2, 4, 6, 8, and 10.